COMPUTER METHODS IN MATERIALS SCIENCE

2022, vol. 22, no. 1, 7–12
https://doi.org/10.7494/cmms.2022.1.0772

Finite element analysis of bipolar plate stamping based on a Yld2000 yield model

Wenyao Wang, Yao Xiao, Nan Guo, Junying Min*

School of Mechanical Engineering, Tongji University, Shanghai 201804, China.

Abstract

Finite element analysis is an essential means for bipolar plate design and the optimization of the manufacturing process. However, the accuracy of the finite element simulation is significantly affected by the constitutive model, especially the yield model. In this paper, uniaxial and biaxial tensile tests were conducted to obtain the yield loci of an ultra-thin austenite stainless steel. The Yld2000 yield model was calibrated using the yield loci under different equivalent plastic strains. The microchannel stamping experiment and its finite element simulations were conducted to study the effect of yield model parameters on the finite element simulation of bipolar plate stamping. The results show that the simulation with Yld2000 calibrated by 0.004 and 0.05 equivalent plastic strain has the best prediction accuracy for the microchannel springback and thickness distribution, respectively.

Keywords: finite element analysis, bipolar plate, yield model, stamping

1. Introduction

A proton exchange membrane fuel cell (PEMFC) is regarded as one of the best candidates to replace traditional power systems due to its high energy density, high conversion rate and zero pollution (Hua et al., 2022; Sim et al., 2018; Wang et al., 2019). The bipolar plate is a critical part of PEMFC, and its forming quality directly affects the performance of the fuel cell. Finite element simulation is a critical step in the bipolar plate design process. As a classical yield model, the Yld2000 yield model (Barlat et al., 2003) has been integrated into the commercial LS-DYNA finite element software, and has been widely used to simulate sheet metal forming. Because more material parameters are required by the Yld2000 yield model during calibration, the prediction accuracy of anisotropic materials under complex strain is obviously higher than other yield models. For some materials, the yield surface evolves with the equivalent plastic strain, such as SS316L, and the yield model parameters calibrated under different equivalent plastic strains differ remarkably. However, many scholars have not considered the influence of different equivalent plastic strains on parameter calibration and simulation accuracy when calibrating Yld2000 yield model parameters. Therefore, it is of great importance to study the effects of the Yld2000 yield model calibrated under different equivalent plastic strains on the simulation of bipolar plate microchannel stamping.

A comprehensive review of anisotropic yield functions is summarised by Banabic et al. (2020) where the recent advanced anisotropic criteria for polycrystalline materials of various crystal structures and experimental

*Corresponding author: junying.min@tongji.edu.cn
ORCID ID's: 0000-0002-9111-004X (W. Wang), 0000-0003-3011-8408 (Y. Xiao), 0000-0003-0905-6310 (N. Guo), 0000-0002-1754-6259 (J. Min)

methods for validating the anisotropic models, including the Biaxial stress test, were introduced. Yong et al. (2017) compared the accuracy of Hill48 (Hill, 1948), Barlat89 (Barlat & Lian, 1989) and Yld2000 (Barlat et al., 2003) yield models in a springback simulation of MP980 U-shaped parts, and the results showed that the eight-parameter Yld2000 yield model had an obvious improvement on the springback prediction accuracy of U-shaped parts. Deng et al. (2017) comparatively studied the influence of a combination of three yield models (Hill48, Barlat89, BBC2005 (Banabic et al., 2005)) and four hardening models (Swift, Ghosh, Hockett–Sherby, Combined S/H-S) on the simulation of AA6016 aluminium alloy forming. The results showed that the yield model was the key factor controlling the simulation accuracy, and the BBC2005 yield model had the highest prediction accuracy, which was in agreement with the experimental value. Pham et al. (2019) modelled the evolution of the Yld2000-2d function as a function of equivalent work, and the material models were applied in finite element simulations to analyse deformation behaviour in uniaxial tension, hydraulic bulge, and punch-stretching tests. The results showed that the model accurately described the material response during these three tests.

In the simulation of bipolar plate stamping, the thinning rate is one of the important indexes to evaluate the formability of the plate under the structure size. The springback determines whether it can meet the requirements of assembling accuracy and working efficiency of the fuel cell stack. The purpose of this study is to investigate the effect of the calibration strategies of the Yld2000 yield model on the simulation accuracy of bipolar plate stamping. An austenite stainless steel 316L with a thickness of 0.1 mm was used in this study. The yield loci of SS316L were obtained through the uniaxial and biaxial tensile tests. A microchannel stamping finite element model was established with the Yld2000 yield model calibrated by different yield loci. With the aid of the microchannel stamping test, the prediction accuracy of the finite element simulation using different Yld2000 yield model parameters was investigated in terms of the cross-section thickness distribution and springback of the microchannel.

2. Finite element simulation

2.1. Yld2000 yield model

Yld2000 yield function was proposed by Barlat et al. (2003), which has eight anisotropy coefficients so that it can accommodate eight mechanical measurements. σ_0, σ_{45}, σ_{90}, R_0, R_{45}, R_{90}, σ_b and R_b are uniaxial tension yield stresses and R values along the RD, DD and TD, as well as the yield stress σ_b and R_b under the balanced biaxial tension condition, respectively.

Its mathematical expression is:

$$\Phi = \Phi'\left(X'\right) + \Phi''\left(X''\right) = 2\bar{\sigma}^a \tag{1}$$

In the formula:

$$\Phi'\left(X'\right) = \left|X_1' - X_2'\right|^a \tag{2}$$

$$\Phi''\left(X''\right) = \left|2X_2'' + X_1''\right|^a + \left|2X_1'' + X_2''\right|^a \tag{3}$$

For face-centred cubic materials, a is 8, $\bar{\sigma}$ is the reference yield stress, X' and X'' are the stress tensors obtained after linear transformation of the partial stress tensor. The elements in X' and X'' can be obtained by a linear transformation of Equation (4):

$$\begin{cases} X' = L'\sigma \\ X'' = L''\sigma \end{cases} \tag{4}$$

The matrix L' and L'' contain eight coefficients $\alpha_1 \sim \alpha_8$ which are related to the anisotropy of the material. The specific values are obtained by fitting R_0, R_{45}, R_{90}, R_b, σ_0, σ_{45}, σ_{90} and σ_b obtained by the biaxial tensile test.

2.2. Finite element model and boundary conditions

The finite element model of microchannel stamping is shown in Figure 1a, the die and punch were rigid, and the blank was deformable. The finite element analysis of the microchannel stamping includes two steps: the stamping through the explicit analysis solver and the springback through the implicit analysis solver. During the springback analysis, the constrain points, as shown in Figure 1b, were selected to eliminate rigid motion. A shell element was used for both the mould and blank. The element size was 0.05 mm × 0.05 mm for the blank and 0.1 mm × 0.1 mm for the molds. A refined grid at the corners and 5 integral points set were constructed in the sheet thickness direction to improve the calculation efficiency while avoiding any loss of accuracy. The details of the finite element analysis are summarised in Table 1.

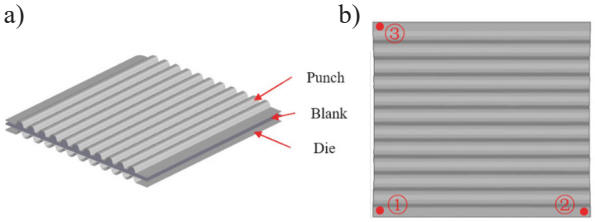

Fig. 1. Finite element model (a) and constrain points selection in springback analysis (b)

Table 1. Finite element boundary condition setting

Software	LSDYNA 9.71 explicit algorithm for stamping; implicit algorithm for springback
Element type	shell for both blank and moulds
Number of through-thickness integration points	5
Element size	0.05 mm by 0.05 mm for blank; 0.1 mm by 0.1 mm for moulds (refine grid at the corners)
Drawing velocity	250 mm/s (Trapezoid)
Friction coefficient	0.1
Contact type	AUTOMATIC_ONE_WAY_SURFACE_TO_SURFACE
Material type	MAT133_BARLAT_YLD2000

3. Experiment

3.1. Uniaxial tensile test

The uniaxial tensile tests were conducted on a MTS E45.105 universal material machine with the digital image correlation (DIC) to obtain the mechanical properties of SS316L. The geometry of specimens was according to the ISO 6892:2016 standard. The specimens were cut along the rolling direction (RD), transverse direction (TD), and diagonal direction (DD) by the electrical discharge machining. Three tests were conducted in each direction to obtain good repeatability results. The loading rate was 3 mm/min for all the tests.

3.2. Biaxial tensile test

The biaxial tensile tests were conducted on a planar biaxial test system MTS BIA5105 to obtain the yield loci of SS316L, which is used to calibrate the Yld2000 model, as shown in Figure 2. The design of the cruciform specimen in this study is based on the standard ISO 16842:2014.

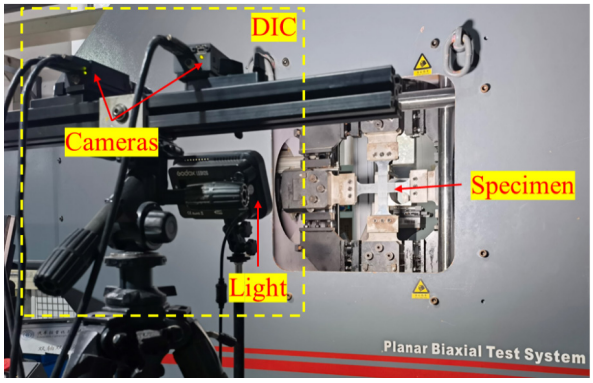

Fig. 2. Biaxial tensile test system

The RD and TD direction of the cruciform specimen is along the *x*-axis and *y*-axis, respectively. The load ratio (*Fx* : *Fy*) was set as 1 : 1. Meanwhile, DIC was applied to obtain the strain on the specimen.

3.3. Microchannel stamping experiment

As shown in Figure 3, the microchannel stamping experiment platform contains the YKP 400 knuckle precision press, microchannel mould, and fixture. In the microchannel stamping tests, the stamping force was set as 400 kN.

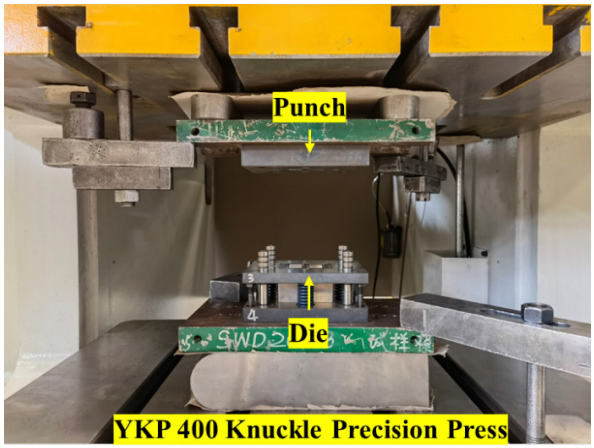

Fig. 3. Microchannel stamping experiment platform

4. Results and discussion

4.1. Experimental results

4.1.1. Uniaxial tensile test results

The mechanical properties obtained from the engineering stress-strain curves are listed in Table 2 and the true stress-strain curves of SS316L along RD, DD, and TD are shown in Figure 4.

Table 2. Mechanical properties of SS316L

Direction	Yield stress σ_0 [MPa]	Tensile strength σ_b [MPa]	Young's modulus E [GPa]	R
RD	326.2	688.0	178.1	0.901
DD	319.4	668.5	183.2	1.043
TD	324.6	665.5	181.7	0.930

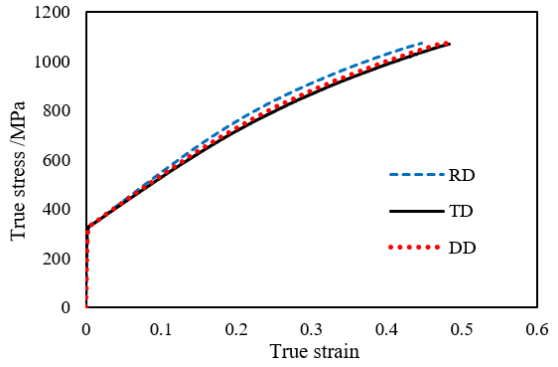

Fig. 4. Uniaxial flow curves of SS316L at three directions

In this paper, the Hockett–Sherby model was used to fit and extend the true stress-plastic strain curve of SS316L. The Hockett–Sherby model expression is shown in Equation (5):

$$\sigma = A + B(1 - \exp(-C \cdot \varepsilon_p^{\ D})) \tag{5}$$

The model parameters A, B, C, and D are 311, 943.47, 3.77, and 1.12, respectively, for SS316L, and the determination coefficient R^2 = 0.99989. Figure 5 exhibits the comparison of the experimental true stress--plastic strain curve along RD and the Hockett–Sherby fitted curve.

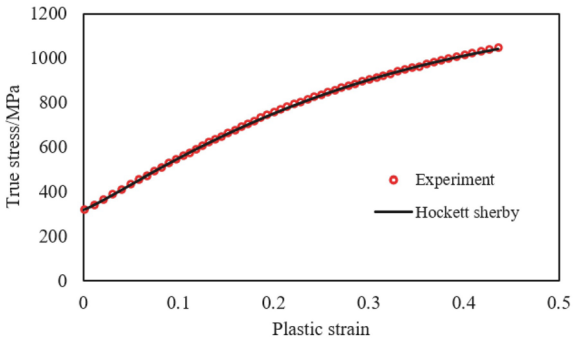

Fig. 5. Fitting curve of Hockett–Sherby hardening model and experimental curve

4.1.2. Experimental results of biaxial tension

The experimental yield loci of SS316L associated with different plastic work per unit volume were obtained, and with increasing plastic work per unit volume, the yield loci of SS316L expanded. The experimental plastic work contours are obtained according to the plastic work equivalent theorem. Figure 6 shows the normalized yield loci of SS316L at 0.002, 0.004, 0.05 and 0.1 equivalent plastic strain. $\bar{\varepsilon}_p$ = 0.002 represents the experimental value at an equivalent plastic strain of 0.002, and Yld2000-0.002 represents the yield loci fitted by the Yld2000 yield model at an equivalent plastic strain of 0.002, the rest are similar. With the increase of equivalent plastic strain, the anisotropy of the yield surface becomes stronger, and the shape of the yield surface tends to be stable when the equivalent plastic strain reaches 0.05. Therefore, the equivalent plastic strain parameters of SS316L yield surface in the initial evolution stage ($\bar{\varepsilon}_p$ = 0.002), the middle evolution stage ($\bar{\varepsilon}_p$ = 0.004) and the stable evolution stage ($\bar{\varepsilon}_p$ = 0.05) were selected for calibration in this paper. Table 3 lists Yld2000 yield model parameters calibrated by R_0, R_{45}, R_{90}, R_b, σ_0, σ_{45}, σ_{90} and σ_b at 0.002, 0.004, and 0.05 equivalent plastic strains.

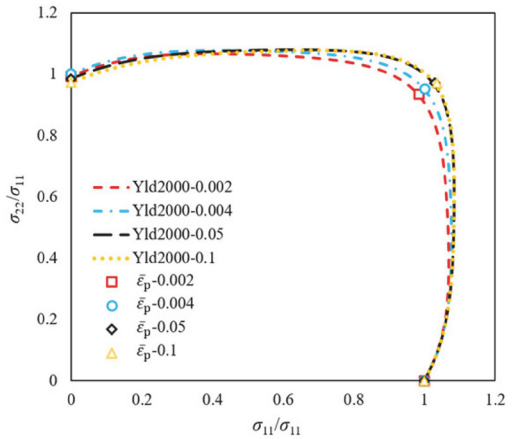

Fig. 6. Yield loci and Yld2000 yield surface of SS316L at various equivalent plastic strains

Table 3. Yld2000 yield model parameters under different equivalent plastic strains (exponent a = 8)

Equivalent plastic strain	α_1	α_2	α_3	α_4	α_5	α_6	α_7	α_8
0.002	0.984	1.021	1.084	1.025	1.022	1.076	1.025	0.983
0.004	0.992	1.002	1.056	1.014	1.013	1.037	1.015	0.985
0.5	0.950	1.060	0.959	1.015	1.005	0.985	1.023	1.050

4.2. Finite element simulation results

4.2.1. Thickness distribution of microchannel cross-section

The thickness distribution on the cross-section of the stamped microchannel was measured using a Keens VHX-5000 Digital Microscope, as shown in Figure 7. The thickness distribution was also extracted from the finite element simulation and compared with the experiment values, as shown in Figure 8. In both the experiment and the finite element simulation, the largest thinning always occurs at the corner of the channel, because the friction force at the corner restricts the material flow. For the thickness of corners 4 and 6, the Yld2000-0.05 provides the most accurate prediction, and the Yld2000-0.002's forecast deviates from the experimental value obviously. In addition, the material deformation at other positions is relatively small, so the simulation is in general agreement with the experiment. In conclusion, the Yld2000 yield model calibrated with 0.05 equivalent plastic strain has a higher prediction accuracy for the thickness distribution of the microchannel.

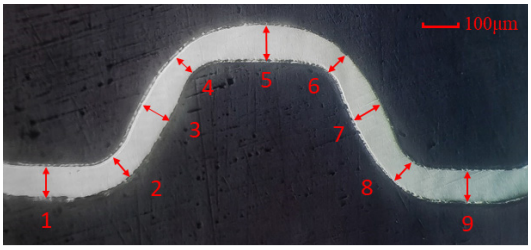

Fig. 7. Microchannel section

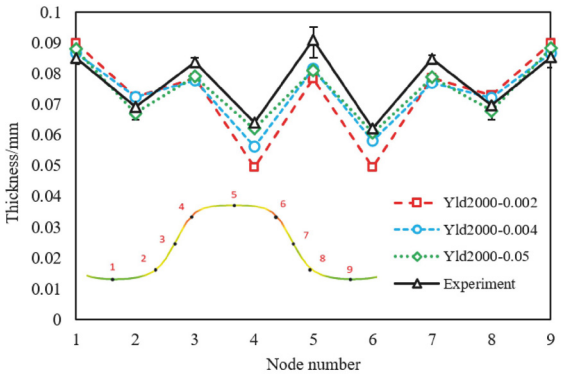

Fig. 8. Thickness distribution of microchannel section

4.2.2. Springback of microchannel

The springback of the stamped microchannel was measured using a Keens VR-5000 3D Optical Profilometer. The coordinates of the centre point at the bottom of each microchannel were selected to characterise the springback. The simulation results are compared with the experimental results in Figure 9. Yld2000-0.002 predicts the maximum springback amount of microchannel, and the maximum displacement in Z direction reaches 0.470 mm, which is much higher than the experimental value of 0.338 mm. The simulation result of Yld2000-0.05 is smaller than the experimental value, while the Yld2000-0.004 provides the most accurate prediction. In conclusion, the Yld2000 yield model calibrated with 0.004 equivalent plastic strain has a higher prediction accuracy for the springback of the microchannel.

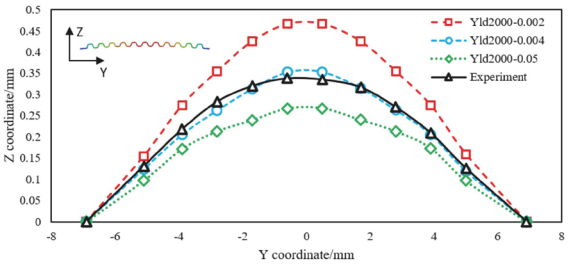

Fig. 9. Comparison between the predicted value and experimental value of microchannel springback under different equivalent plastic strains

5. Conclusion

In this paper, the yield loci of an austenite stainless steel 316L were obtained from the uniaxial and biaxial tensile tests. The Yld2000 yield model was calibrated via the yield loci at different equivalent plastic strains. The effect of Yld2000 model parameters on the accuracy of microchannel stamping finite element simulation was investigated in terms of the cross-section thickness distribution and springback, and the following conclusions can be drawn here:

- The yield surface of SS316L evolves with the increase of the equivalent plastic strain, and the shape of the yield surface tends to be stable when the equivalent plastic strain reaches 0.05.
- The material model parameters have a significant influence on FE simulation. Yld2000-0.05 provide the most accurate result for the thickness distribution, and Yld2000-0.004 provide the most accurate result for the springback of the microchannel.

Acknowledgements

The authors would like to acknowledge the financial support for this research provided through the National Key Research and Development Program of China (No. 2020YFB1505900).

References

Banabic, D., Aretz, H., Comsa, D.S., & Paraianu, L. (2005). An improved analytical description of orthotropy in metallic sheets. *International Journal of Plasticity*, *21*(3), 493–512. https://doi.org/10.1016/j.ijplas.2004.04.003.

Banabic, D., Barlat, F., Cazacu, O., & Kuwabara, T. (2020). Advances in anisotropy of plastic behaviour and formability of sheet metals. *International Journal of Material Forming*, *13*(5), 749–787. https://doi.org/10.1007/s12289-020-01580-x.

Barlat, F., & Lian, K. (1989). Plastic behavior and stretchability of sheet metals. Part I: A yield function for orthotropic sheets under plane stress conditions. *International Journal of Plasticity*, *5*(1), 51–66. https://doi.org/10.1016/0749-6419(89)90019-3.

Barlat, F., Brem, J.C., Yoon, J.W., Chung, K., Dick, R.E., Lege, D.J., Pourboghrat, F., Choi, S.-H., & Chu, E. (2003). Plane stress yield function for aluminum alloy sheets – part 1: theory. *International Journal of Plasticity*, *19*(9), 1297–1319. https://doi.org/10.1016/S0749-6419(02)00019-0.

Deng, Z., & Hennig, R. (2017). Influence of material modeling on simulation accuracy of aluminum stampings. *Journal of Physics: Conference Series. 896*(1), 012025. https://doi.org/10.1088/1742-6596/896/1/012025.

Hill, R. (1948). A theory of the yielding and plastic flow of anisotropic metals. *Proceedings of the Royal Society of London. Series A. Mathematical and Physical Sciences*, *193*(1033), 281–297. https://doi.org/10.1098/rspa.1948.0045.

Hou, Y., Min, J., Lin, J., Liu, Z., Carsley, J.E., & Stoughton, T.B. (2017). Springback prediction of sheet metals using improved material models. *Procedia Engineering*, *207*, 173–178. https://doi.org/10.1016/j.proeng.2017.10.757.

Hua, R., Zhang, W., & Cheng, L. (2022). Review on Design and Forming Technology of Metallic Bipolar Plates for Fuel Cells. *Journal of Netshape Forming Engineering*, *14*(3), 25–33. https://doi.org/10.3969/j.issn.1674-6457.2022.03.004.

ISO 16842:2014. Metallic materials – Sheet and strip – Biaxial tensile testing method using a cruciform test piece.

ISO 6892-1:2016. Metallic materials – Tensile testing. Part 1: Method of test at room temperature.

Pham, Q.T., Lee, M.G., & Kim, Y.S. (2019). Characterization of the isotropic-distortional hardening model and its application to commercially pure titanium sheets. *International Journal of Mechanical Sciences*, *160*, 90–102. https://doi.org/10.1016/j.ijmecsci.2019.06.023.

Sim, Y., Kwak, J., Kim, S.Y., Jo, Y., Kim, S., Kim, S.Y., Kim, J.H., Lee Ch.S., Jo, J.H., & Kwon, S.Y. (2018). Formation of 3D graphene – Ni foam heterostructures with enhanced performance and durability for bipolar plates in a polymer electrolyte membrane fuel cell. *Journal of Materials Chemistry A*, *6*(4), 1504–1512. https://doi.org/10.1039/C7TA07598G.

Wang, L., Tao, Y., Zhang, Z., Wang, Y., Feng, Q., Wang, H., & Li, H. (2019). Molybdenum carbide coated 316L stainless steel for bipolar plates of proton exchange membrane fuel cells. *International Journal of Hydrogen Energy*, *44*(10), 4940–4950. https://doi.org/10.1016/j.ijhydene.2018.12.184.